

Article

Evaluation of Hydrogen Permeation into High-Strength Steel during Corrosion in Different Marine Corrosion Zones

Yong Xu^{1,2,3,4}, Yanliang Huang^{1,2,4,*} , Fanfan Cai^{1,2,3,4}, Zhengquan Wang^{1,2,3,4}, Dongzhu Lu^{1,2,4} ,
Xiutong Wang^{1,2,4}  and Lihui Yang^{1,2,4}

¹ CAS Key Laboratory of Marine Environmental Corrosion and Bio-Fouling, Institute of Oceanology, Chinese Academy of Sciences, Qingdao 266071, China; xuyong182@mails.ucas.ac.cn (Y.X.); caifanfan20@mails.ucas.ac.cn (F.C.); 17854268797@163.com (Z.W.); ldz@qdio.ac.cn (D.L.); wangxiutong@qdio.ac.cn (X.W.); lhyang@qdio.ac.cn (L.Y.)

² Open Studio for Marine Corrosion and Protection, Pilot National Laboratory for Marine Science and Technology, Qingdao 266237, China

³ University of Chinese Academy of Sciences, Beijing 100049, China

⁴ Center for Ocean Mega-Science, Chinese Academy of Sciences, 7 Nanhai Road, Qingdao 266071, China

* Correspondence: hyl@qdio.ac.cn

Abstract: Hydrogen permeation into high-strength steel during the corrosion process can deteriorate their mechanical properties, thus seriously threatening the safety of steel structures. However, the hydrogen permeation behavior of steels in corrosive marine environments is not well understood. In this study, the hydrogen permeation behavior and mechanism of AISI 4135 steel in different marine corrosion zones was investigated for the first time using an in situ hydrogen permeation monitoring system via outdoor and indoor tests. The three-month outdoor hydrogen permeation test showed that the diffusible hydrogen content of the steels exposed to the marine atmospheric, splash, tidal and immersion zone was 3.15×10^{-3} , 7.00×10^{-2} , 2.06×10^{-2} and 3.33×10^{-2} wt ppm, respectively. Meanwhile, results showed that the hydrogen permeation current density was positively correlated with the corrosion rate of the steel in the marine environments. This research is of great significance for guiding the safe application of high-strength steel in the marine environments.

Keywords: high-strength steel; hydrogen permeation; sensor; marine corrosion environments



Citation: Xu, Y.; Huang, Y.; Cai, F.; Wang, Z.; Lu, D.; Wang, X.; Yang, L. Evaluation of Hydrogen Permeation into High-Strength Steel during Corrosion in Different Marine Corrosion Zones. *Appl. Sci.* **2022**, *12*, 2785. <https://doi.org/10.3390/app12062785>

Academic Editors: Giuseppe Lacidogna, Sanichiro Yoshida, Guang-Liang Feng, Jie Xu, Alessandro Grazzini and Gianfranco Piana

Received: 29 January 2022

Accepted: 28 February 2022

Published: 9 March 2022

Publisher's Note: MDPI stays neutral with regard to jurisdictional claims in published maps and institutional affiliations.



Copyright: © 2022 by the authors. Licensee MDPI, Basel, Switzerland. This article is an open access article distributed under the terms and conditions of the Creative Commons Attribution (CC BY) license (<https://creativecommons.org/licenses/by/4.0/>).

1. Introduction

With the development of the iron and steel manufacturing industry, high-strength steel has been gradually used in various industries such as civil buildings, energy transportation and marine engineering due to its superior mechanical properties. However, high-strength steel endures severe corrosion and other potential threats during its service in offshore engineering facilities, owing to the harsh marine environments. Among these threats, the mechanical degradation of steel caused by hydrogen permeation during the corrosion process has received widespread attention in the last few decades [1–4]. Wang et al. [4] found that diffusible hydrogen led to a decrease in the notch tensile strength for the AISI 4135 steels at 1320 MPa in a power law manner. Liu et al. [5] found that E690 steel exhibited high susceptibility to stress corrosion cracking (SCC) under simulated marine thin electrolyte layer and indicated that the SCC process was jointly determined by local anodic dissolution (AD) and hydrogen embrittlement (HE). Li et al. [6] found that the change in fracture stress of steels showed apparent correspondence with the change in hydrogen content during the evaluation on delayed fracture property of outdoor-exposed high-strength AISI 4135 steels. To date, it has been recognized that hydrogen plays a critical role in the fracture failure of steels, while the sensitivity of steels to hydrogen increases sharply with strength [7,8].

Generally, there are two main sources of hydrogen permeated into steels: a part of hydrogen comes from the steel production and subsequent processing process, such as

pickling and plating; while most of the hydrogen absorbed into steel comes from the corrosion processes, especially the hydrolysis of corrosion products [9,10]. It has been found that hydrogen permeation behavior into steel is closely related to the corrosion behavior of steel [11–16]. Our previous studies [11,12] found that the amount of hydrogen permeated into steel is positively correlated with the corrosion weight loss of steel under the simulated wet–dry cycle condition. Meanwhile, the positive relationship between the hydrogen permeation and steel corrosion in the automobile moving environment and the atmospheric corrosion environment has also been reported in previous studies [13,14]. Furthermore, it is well known that the amount of hydrogen permeated into steel increases significantly in the case of salts being loaded on the surface of steels [9,15,16]. Therefore, hydrogen permeation behavior into steel should be more serious and complex in the marine corrosive environments according to above analysis. Traditionally, the marine corrosive environments are divided into five zones including the marine atmospheric zone, the splash zone, the tidal zone, the full immersion zone and the seabed sediment zone [17]. For offshore facilities, the steel structures run through different corrosion zones, and the hydrogen permeation behavior caused by varying degrees of corrosion may also be diverse at different locations.

Since the amount of hydrogen permeated into steel plays an essential role in the hydrogen embrittlement or delayed fracture of steel, it is significant to clarify how much hydrogen can be permeated into steel during service in a certain environment [17,18]. Over the past few decades, important progress has been made on understanding the hydrogen permeation behavior of steel in atmospheric environments [14,19–21], but relevant information on such behavior of steel in more complex and harsh marine environments remains limited. Therefore, systematic and scientific research should be carried out on the hydrogen permeation behavior of steels in marine environments. Among the methods for the determination of hydrogen content in steel, the electrochemical hydrogen permeation technique is widely used in various scenarios due to its excellent reliability and adaptability [22–24]. In this work, the electrochemical hydrogen permeation test was performed in outdoor marine environments using an in situ monitoring system developed by the authors to investigate the hydrogen permeation behavior of AISI 4135 steel in different marine corrosion zones. In addition, combined with a laboratory test, the hydrogen permeation mechanism of steels in marine environments was analyzed.

2. Materials and Methods

2.1. Material and Outdoor Test Site

The material used in this work was as-received AISI 4135 high-strength steel produced by Beijing Shougang New Steel Co., Ltd., Beijing, China, and its chemical composition is provided in Table 1. The mechanical properties include a tensile strength of 830 MPa, a yield strength of 780 MPa and an elongation of 10.4% at ambient temperature (20 °C). To observe the microstructure of the steel, a steel sample of 10 mm in diameter and 10 mm in height was ground with a series of silicon carbide (SiC) papers (from 400 to 1000 grade) and then polished with a 2.5 µm diamond abrasive. Then, the sample was etched in a nital etchant (4% nitric acid and 96% anhydrous alcohol) for 10 s, treated with deionized water, swabbed with alcohol and finally dried in a cold air stream. The microstructure of the AISI 4135 high-strength steel is shown in Figure 1, where pearlite and ferrite can be observed. The specimens are hollow cylindrical steels with open ends, an inner diameter of 34 mm and a wall thickness of 0.5 mm (See Figure S1 for more information on the dimensions of the specimens). Both the inner and outer surfaces of the cylindrical wall were grinded, with a final roughness average (Ra) of 0.4. A palladium (Pd) film of ca. 0.6 µm in thickness was electroplated on the inner surface of the hollow cylindrical steel for facilitating hydrogen detection, inhibiting corrosion, etc. [25–27]. The effective hydrogen diffusion coefficient, D_{eff} , of the specimen was determined through the breakthrough-time method [28], the value of which was $4.13 \times 10^{-7} \text{ cm}^2 \cdot \text{s}^{-1}$. The outdoor hydrogen permeation test was conducted in Xuejia Island Harbor (36°06' N; 120°10' E), Qingdao, China. The tide in the sea area is

of typical semidiurnal one, and the record shows that the annual average tidal range and temperature were ~ 2.7 m and ~ 12 °C, respectively.

Table 1. Chemical composition of the AISI 4135 steel used in this work (wt.%).

C	Si	Mn	P	S	Ni	Cr	Mo	Fe
0.399	0.293	0.509	0.0146	0.0144	0.0804	0.903	0.204	Bal.

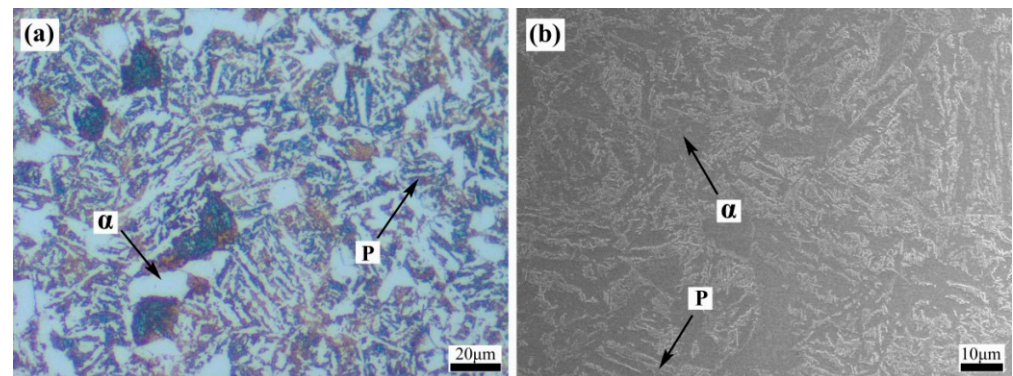


Figure 1. Microstructure of AISI 4135 high-strength steel: OM micrograph (a), SEM micrograph (b); α —Ferrite, P—Pearlite.

2.2. In Situ Hydrogen Permeation Monitoring Test

2.2.1. In Situ Hydrogen Permeation Monitoring Set-Up

In this study, the hydrogen permeated into the hollow cylindrical steel specimen during exposure to the marine environments was monitored in situ using the hydrogen permeation monitoring set-up shown in Figure 2. Based on Devanathan–Stachurski technique [29], the developed set-up can evaluate the hydrogen permeated into steel via measuring the so-called “anodic oxidation current”. To make it clear, the set-up shown in Figure 2 is referred to “hydrogen permeation sensor” and unless otherwise specified, the sensor mentioned below is a hydrogen permeation sensor. Inside the sensor was a closed three-electrode system: the inner surface of the hollow cylindrical steel specimen was the working electrode, a Pt wire as counter electrode, a Hg/HgO/0.2 mol/L NaOH electrode as reference electrode and the nitrogen deaerated 0.2 mol/L NaOH + 30 vol% dimethyl sulfoxide (DMSO) solution as the inner electrolyte. The outer surface of the sensor was sealed with custom-built poly tetra fluoroethylene (PTFE) shells and epoxy resin except for the area reserved for exposure, as shown in Figure 2. During hydrogen permeation test, the inner surface with Pd-plated acted as so-called “hydrogen detection side”; while the outer surface of the sensor exposed to the marine environments acted as so-called “hydrogen entry side”. The multi-core copper wires connecting the electrodes were led out through a waterproof connector, and the wire joints were sealed with epoxy resin inside the sensor.

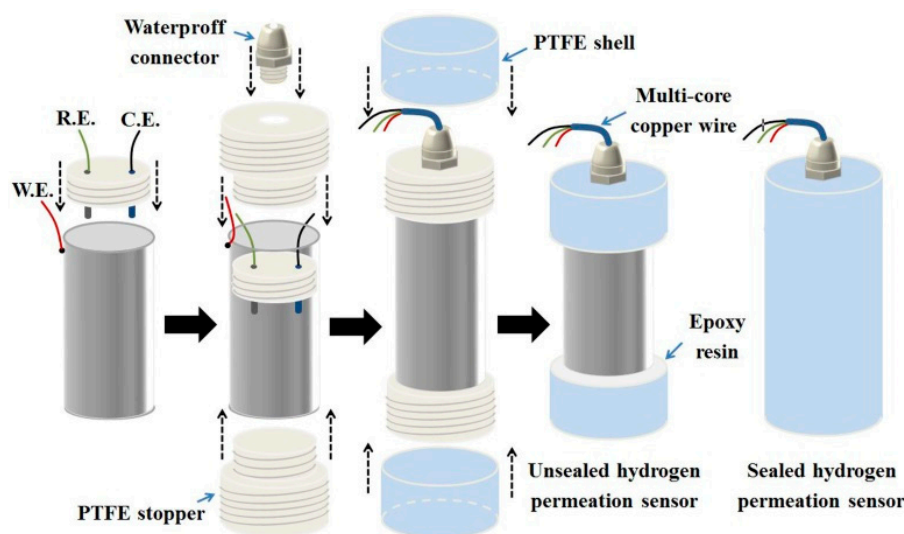


Figure 2. Schematic diagram of the hydrogen permeation sensor.

Before the in situ hydrogen permeation monitoring test, the Pd-plated surface of the sensor was polarized at 0 mV (vs. Hg/HgO) and left for at least 24 h to ensure the polarization current density monitored decreased to below $0.1 \mu\text{A}\cdot\text{cm}^{-2}$. In addition, as shown in Figure 2, the sensor whose outer surface was fully sealed with epoxy resin and PTFE shell served as a control sample, for correcting the background current fluctuations caused by temperature variations. This control sample is also referred to as a completely sealed sensor in later sections. Since no surface of the steel was exposed to corrosive media because of the covering by epoxy resin and PTFE, it is regarded that there is not an electrochemical reaction (including corrosion reaction) occurring on the surface of the completely sealed sensor.

2.2.2. In Situ Hydrogen Permeation Monitoring Test in the Outdoor Marine Environments

The in situ hydrogen permeation monitoring test was carried out to investigate the hydrogen permeation behavior into steel in outdoor marine environments. During the test, sensors were individually suspended on an insulated wire rope and fixed at different positions in the vertical direction of the sea by clamps. The hydrogen permeation sensor was connected to a multi-channel Potentiostat (made in Japan) via copper wires. Meanwhile, a temperature sensor was installed near the hydrogen permeation sensor to monitor temperature changes. According to the tidal record of the experimental sea area, the position distribution of the sensors in the vertical direction of the sea was determined, including the marine atmospheric zone, the splash zone, the tidal zone and the immersion zone. Details of the position distribution of the sensors along the vertical direction of the sea are shown in Figure 3.

As a blank control, the completely sealed sensor was suspended alone on another insulated wire rope and placed side by side with the sensor exposed to the marine atmospheric zone. Tide heights were monitored in real time through a pressure sensor placed at the bottom of the immersion zone. Both the tidal data and above temperature data were recorded by a HIOKI MEMORY HILOGGER. In addition, due to the important influence of humidity on the corrosion of steel in the atmospheric zone, the changes in marine atmospheric humidity were also monitored and recorded by a hygrothermograph. The in situ hydrogen permeation monitoring test started on 6 July 2020, and ended on 12 October 2020, a period encompassing the summer and early autumn of the Northern hemisphere.

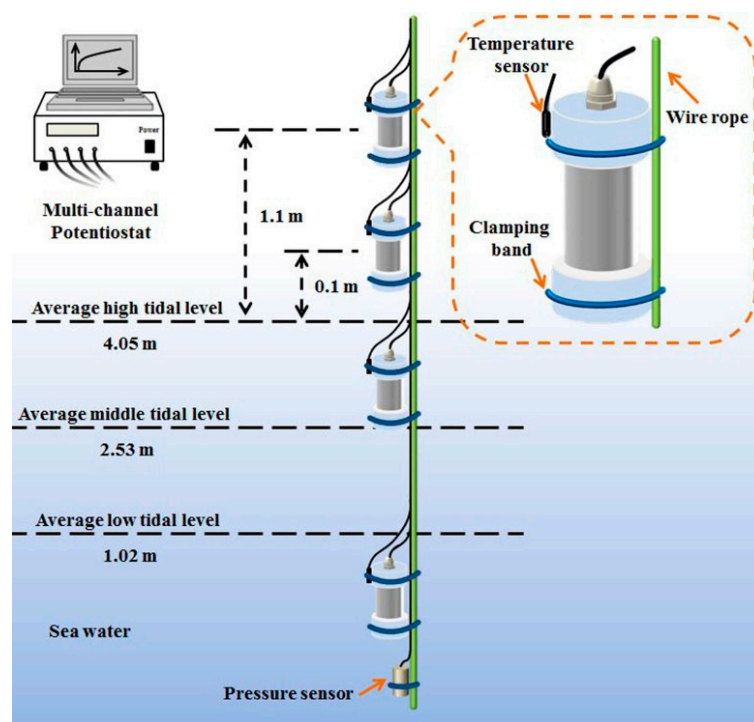


Figure 3. Schematic diagram of the outdoor hydrogen permeation test.

2.2.3. Measurement of Corrosion Thickness Loss

The hydrogen permeation sensor was also used as a corrosion coupon. The parameter of corrosion thickness loss was adopted to quantify the corrosion degree of sensors after outdoor exposure. The hydrogen permeation sensor was cut into two sections from the middle with a hacksaw. One section of the sensor was sealed with epoxy resin, and then the cross-section of the sensor was grinded with SiC paper up to 1000 grade. Subsequently, it was polished with a 3 μm diamond abrasive and then rinsed with distilled water and alcohol to obtain a smooth surface for observation. Measurement of the residual thickness of the sensor wall was performed with a Jangnan MR-2000 optical metallographic microscope and accompanying software of ScopeImage 9.0.

2.2.4. Analysis of Corrosion Products

The corrosion product layers scraped from the sensors were grinded to fine powders and then analyzed by using X-ray diffraction (XRD) and Raman spectroscopy. XRD patterns were obtained with an Ultima IV X-ray diffractometer with Cu K α radiation ($\lambda = 1.5406 \text{ \AA}$) operating at 40 kV and 40 mA. The 2θ ranged from 5° to 80° at a scanning rate of 2° min^{-1} and the data were processed with software of MDI Jade 6.5. Raman analysis was performed on a micro-Raman spectrometer (Renishaw MZ20-FC) equipped with a solid-state diode pumped green laser (wavelength $\lambda = 532 \text{ nm}$), and the Raman shift range was $0\sim 1800 \text{ cm}^{-1}$.

2.3. Indoor Simulated Hydrogen Permeation Test

To investigate the hydrogen permeation behavior and mechanism of the steel under a wet–dry cycle condition, a hydrogen permeation test was carried out in a simulated tidal cycling condition in the laboratory. The simulated tidal cycles were realized through a platform and water tank that can be regularly raised and lowered, as shown in Figure 4. The indoor tidal cycles simulate semidiurnal tides, which were 6 h of immersion in sea water, then 6 h of air exposure, and so on. During the indoor hydrogen permeation monitoring tests, in addition to the continuous monitoring of hydrogen permeation behavior, open circuit potential (OCP) of the steel was continuously monitored through a calomel electrode which was always immersed in sea water. A cotton thread is connected between the sensor

and the water tank to ensure that the OCP of the sensor can be continuously monitored during tidal cycles. Meanwhile, the potential between the sensor and another calomel electrode fixed on the sensor was continuously monitored, as an indicator potential to indicate the drying or wetting stage.

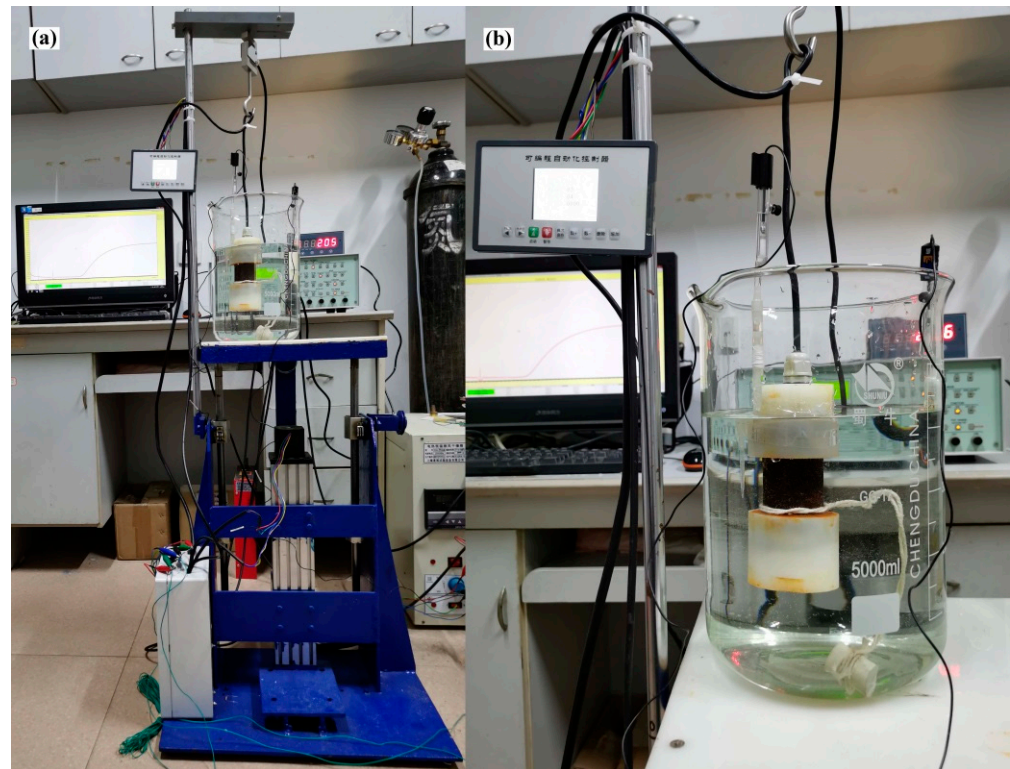


Figure 4. Photos of the hydrogen permeation test set-up under simulated tidal cycling condition in laboratory (a), enlarged view of electrolytic cell (b).

3. Results and Discussion

3.1. Hydrogen Permeation Monitoring Test in the Outdoor Marine Environments

3.1.1. Hydrogen Permeation Behavior of Steels in Different Marine Corrosion Zones

Figure 5 shows the macro-morphologies of sensors after being exposed for 3 months in outdoor marine environments. It can be seen that the sensors exposed to different corrosion zones endured varying degrees of corrosion. The sensor exposed to the marine atmospheric zone was less corroded in comparison with the sensors exposed to other corrosion zones. Meanwhile, the sensor exposed to the tidal zone was obviously affected by biofouling, and the sensor surface was covered with a large number of barnacles (Figure 5c). To date, the effect of macro biofouling on steel corrosion remains controversial. On the one hand, macro-fouling organisms such as oyster, barnacle and filamentous macroalgae may induce crevice corrosion, or accelerate the corrosion process by facilitating the growth of microbial communities, as elaborated in literatures [30–32]; on the other hand, based on outdoor measurement data, it was found that there was a negative relationship between biomass data and corrosion mass loss, suggesting that macro-fouling played a positive role in reducing mass loss [33,34]. In addition, due to the scouring action of sea water and prolonged immersion, it was observed that the rust layer formed on the surface of the sensor exposed to the immersion zone was relatively loose, and the surface was covered with silt-like sediments. Given the positive relationship between hydrogen permeation and corrosion of steel, varying degrees of corrosion for steel may imply differences in the amount of hydrogen permeated into the steel.

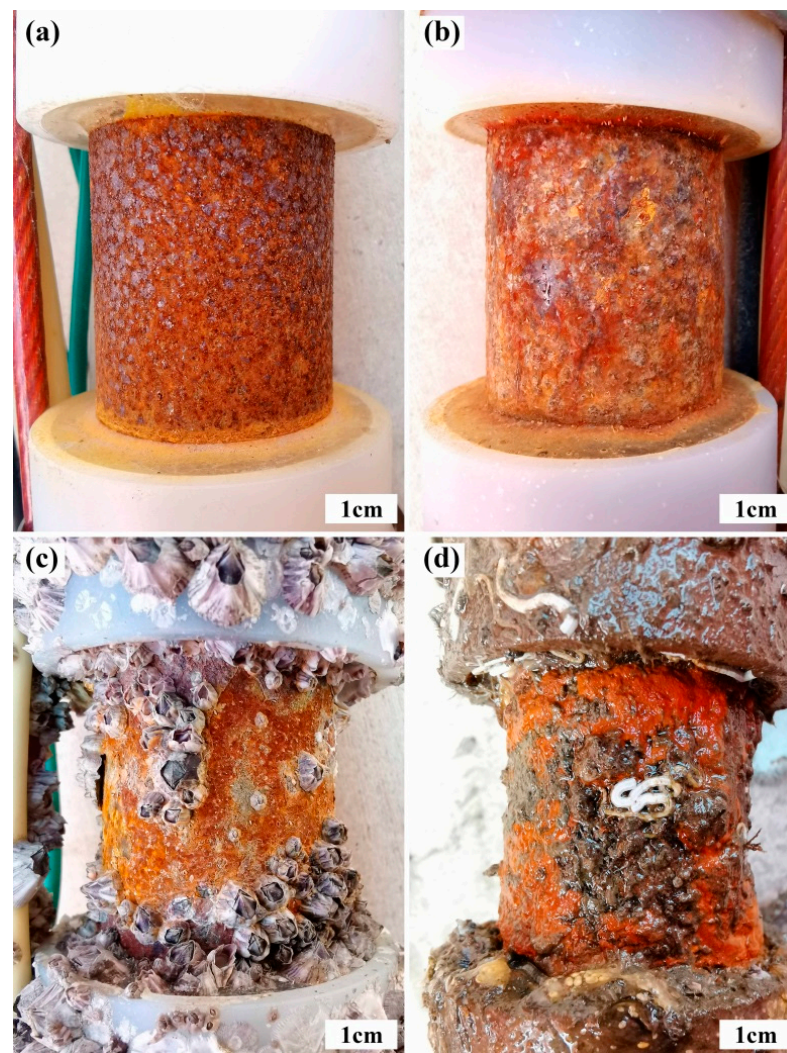


Figure 5. Macro-morphologies of the sensors after being exposed for 3 months in the marine atmospheric zone (a), the splash zone (b), the tidal zone (c) and the immersion zone (d).

Figure 6a shows the polarization current of the completely sealed sensor exposed to the atmospheric zone, and environment temperature from 4 August to 9 August. It is observed that there is a positive relationship between the background current and environment temperature. Since there is no electrochemical reaction (including corrosion reaction) occurring on the surface of the completely sealed sensor, it is considered that the variation of the polarization current density in Figure 6a is caused by temperature change rather than hydrogen permeation. Accordingly, for a sensor that is not completely sealed, the polarization current contributed by hydrogen permeation (i.e., hydrogen permeation current) can be obtained by subtracting the polarization current totally caused by temperature (i.e., background current). In other words, the hydrogen permeation current can be expressed as Equation (1).

$$i_H = i_a - i_b \quad (1)$$

where i_H is the hydrogen permeation current, i_a and i_b are the total anodic polarization current and background current, respectively. Based on a large amount of polarization current data of the completely sealed sensor (i.e., background current data) and temperature data, the quantitative relationship between the background current and temperature was obtained by fitting, as shown in Figure 6b. Accordingly, changes in the background current can be determined via the variation of environment temperature during tests.

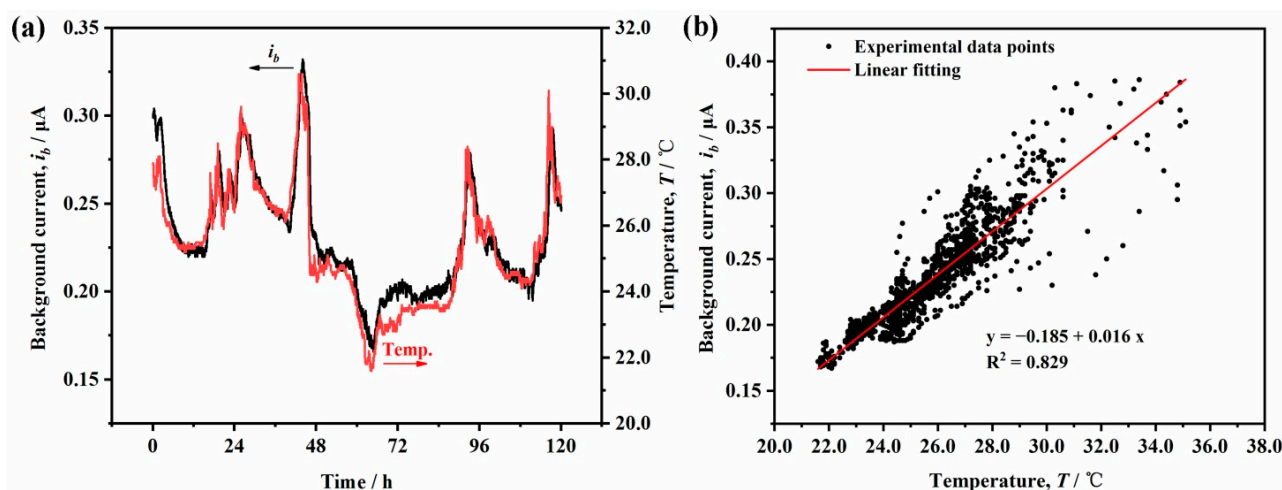


Figure 6. Variations of the background current with environment temperature (a), and the relationship between the background current and environment temperature (b).

Figure 7 shows the hydrogen permeation current of the sensor exposed to the marine atmospheric zone, temperature and relative humidity, as well as weather records, from 4 August to 9 August. The data show that the relative humidity and temperature of the marine atmosphere were relatively high during this period (Figure 7a), which provided favorable conditions for the corrosion of steel in the marine atmospheric zone. It is seen that the hydrogen permeation current increases significantly when the temperature rises. On one hand, the increase in temperature facilitates the corrosion of the steel, thereby promoting hydrogen permeation into steel [13]; on the other hand, an increased temperature can increase the H diffusion activation energy, leading to more hydrogen permeation into steel, which may also be a reason for the increased hydrogen permeation current [35,36]. In addition, it is found that the hydrogen permeation current is generally low, when it is rainy. The apparent decrease in hydrogen permeation current during rainfall can be attributed to both the loss of pollutions deposited on the steel surface and the decrease in temperature. It is well known that pollutions such as Cl^- and SO_2 have an accelerated effect on the corrosion of steel, so that the corrosion rate of steel decreases as pollutions are washed off from steel surface when it rains [37]. Meanwhile, it can be seen in later discussions that the hydrogen permeation current has a positive relationship with the corrosion rate due to the hydrolysis of the corrosion products, hence a lower corrosion rate corresponds to a lower hydrogen permeation current. Accordingly, for steels being exposed to the marine atmospheric zone, pollutions deposition and salts loading which are related to the humidity and weather conditions also play an important role in hydrogen permeation behavior.

Figure 8 shows transients of the hydrogen permeation current density of the sensor exposed to the splash zone, and changes in temperature and tide. Taking the position of the pressure sensor in the full immersion zone as the reference zero point, the specific position of the sensor in the splash zone is as shown in Figure 8b. A large hydrogen permeation current density was observed, with the value approximately 10 times that of the current density for the sensor exposed to the marine atmospheric zone (Figures 7a and 8a). It is well known that steel exposed to the splash zone is prone to endure more severe corrosion [38,39]. Therefore, a large hydrogen permeation current of the steel exposed to the splash zone is reasonable, according to the positive relationship between corrosion of steel and hydrogen permeation. For steel exposed to the splash zone, the wet–dry alternation of the steel surface is mainly controlled by splashing waves. It can be observed that the hydrogen permeation current was relatively high when the surface of the steel was in a wetting stage caused by spindrift, suggesting a corrosion accelerated process in the wetting stage. Furthermore, the promoting effect of a high temperature on hydrogen permeation was more obvious in the splash zone, on the basis of a higher hydrogen permeation current, as shown in Figure 8a.

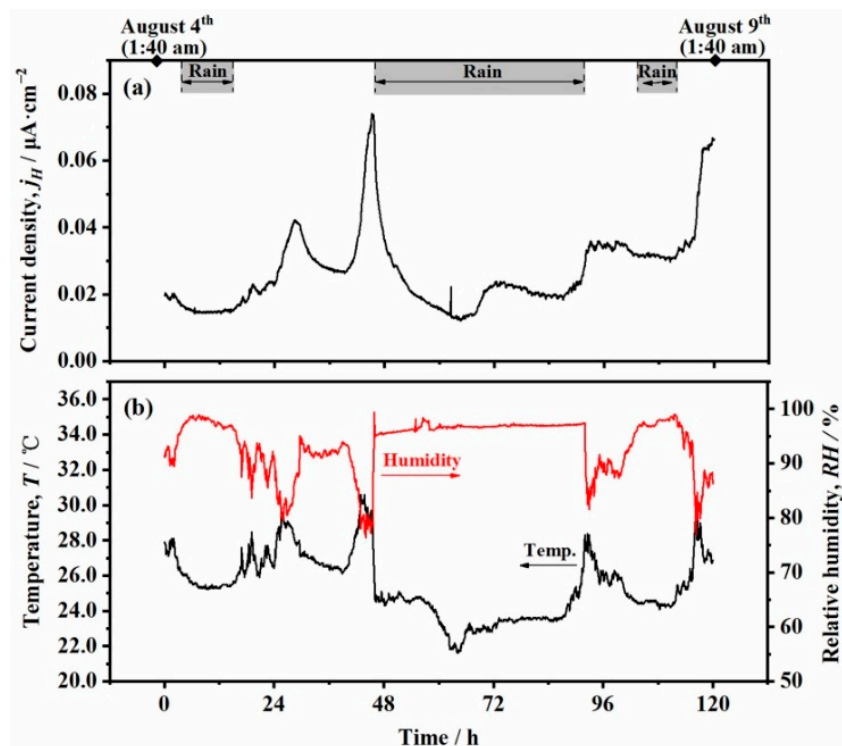


Figure 7. Time variations of the hydrogen permeation current density of the sensor exposed to the marine atmospheric zone (a), and temperature/relative humidity changes (b) from 4 August to 9 August during outdoor hydrogen permeation test.

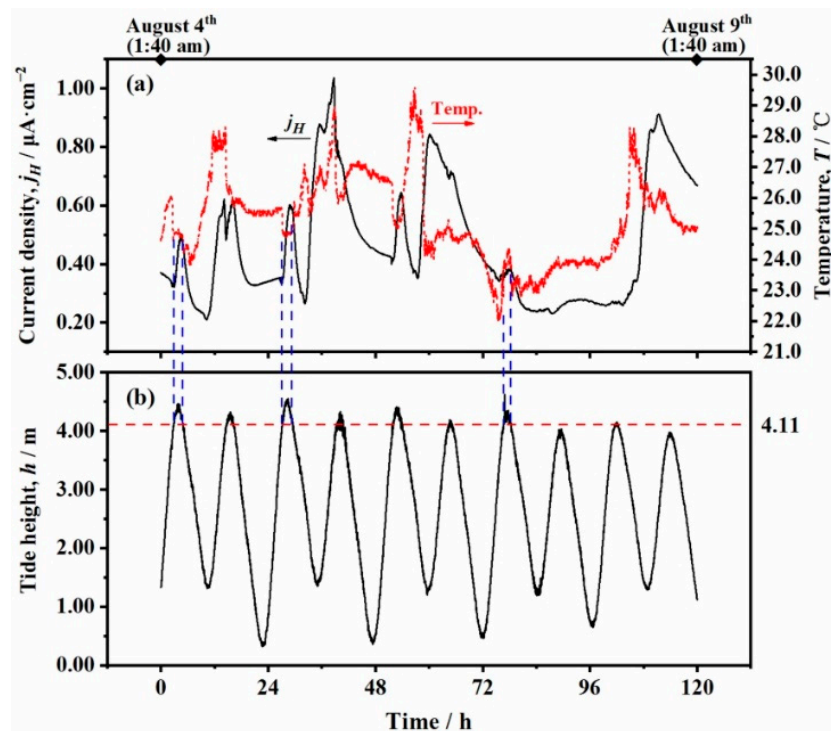


Figure 8. Time variations of the hydrogen permeation current density of the sensor exposed to the splash zone and the corresponding temperature (a), as well as tidal changes (b) from 4 August to 9 August during outdoor hydrogen permeation test.

Figure 9 shows transients of the hydrogen permeation current density of the sensor exposed to the splash zone, and changes in temperature and tide. The specific position of

the sensor exposed to the tidal zone is shown in Figure 9b. The obvious fluctuations of temperature with tides were observed in Figure 9a, owing to the difference in the specific heat capacity between sea water and air, as well as the evaporation of water. Meanwhile, a current peak was observed in each tidal cycle. It is believed that the appearance of current peak is related to the temperature effect on the one hand and may be related to the difference in the cathodic reactions between drying and wetting process on the other hand (details refer to Section 3.2). Furthermore, it was also found that the hydrogen permeation current of the sensor exposed to the tidal zone was approximately one quarter that of the sensor exposed to the splash zone. This indicates that the corrosion of steel in the tidal zone is relatively light in comparison with that of steel in the splash zone.

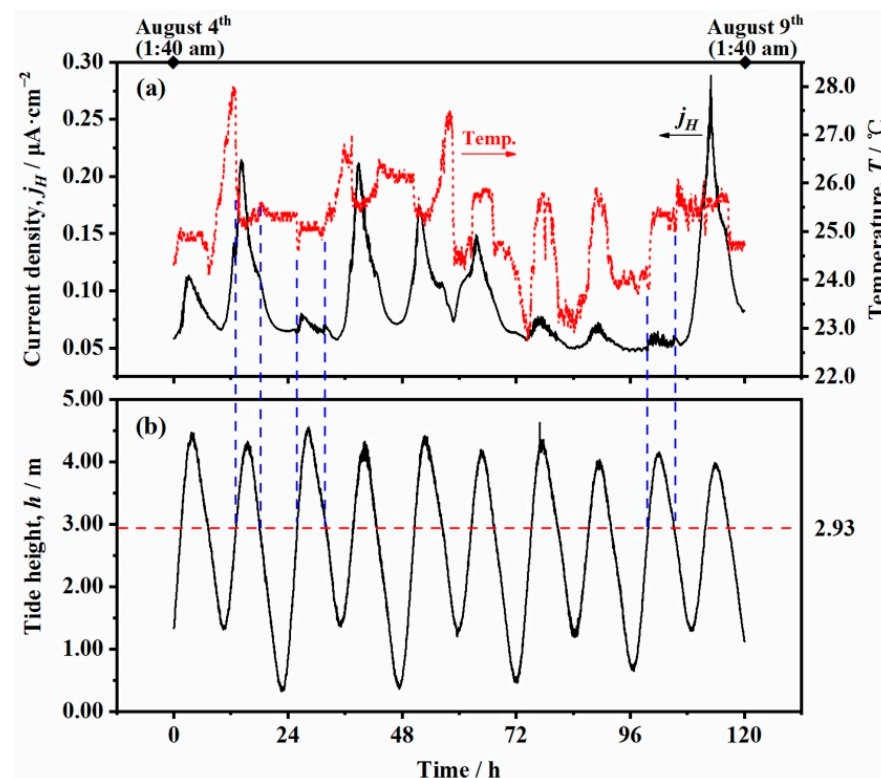


Figure 9. Time variations of the hydrogen permeation current density of the sensor exposed to the tidal zone and the corresponding temperature (a), as well as tidal changes (b) from 4 August to 9 August during outdoor hydrogen permeation test.

Figure 10a shows transients of the hydrogen permeation current density of the sensor exposed to the immersion zone and temperature. It can be seen that the hydrogen permeation current of the sensor exposed to the immersion zone was much larger than that of the sensor exposed to the tidal zone. The relatively large hydrogen permeation current in the immersion zone may be caused by the stronger reproduction and metabolic activity of sulfate-reducing bacteria (SRB) on the surface of the steel in the immersion zone. It can be observed that part of the surface of the hydrogen permeation sensor in the immersion zone was covered by a layer of gray-black sediments, both the sediments and relatively low concentration of dissolved oxygen in the immersion zone providing favorable living conditions for SRB. Raman spectroscopy shown in Figure 11b confirmed that the presence of ferrous sulfide (FeS) in the corrosion products formed in the immersion zone, with the characteristic peak at 284 cm^{-1} [40]. The formation of FeS is related to the activities of SRB, and published study showed that SRB were tend to be present in the inner black stratum of the corrosion products layer [41]. Meanwhile, sulfate green rust [GR(SO₄²⁻)], akaganeite (β -FeOOH) and magnetite (Fe₃O₄) were also detected in the corrosion products, with the characteristic peaks at 217 cm^{-1} , 385 cm^{-1} and 638 cm^{-1} , respectively [42,43]. However, no

FeS was found in the corrosion products formed in the tidal zone, only β -FeOOH, Fe_3O_4 and lepidocrocite (γ -FeOOH) were detected, with the characteristic peaks at 312 cm^{-1} , 540 cm^{-1} and 706 cm^{-1} , respectively (Figure 11a) [43].

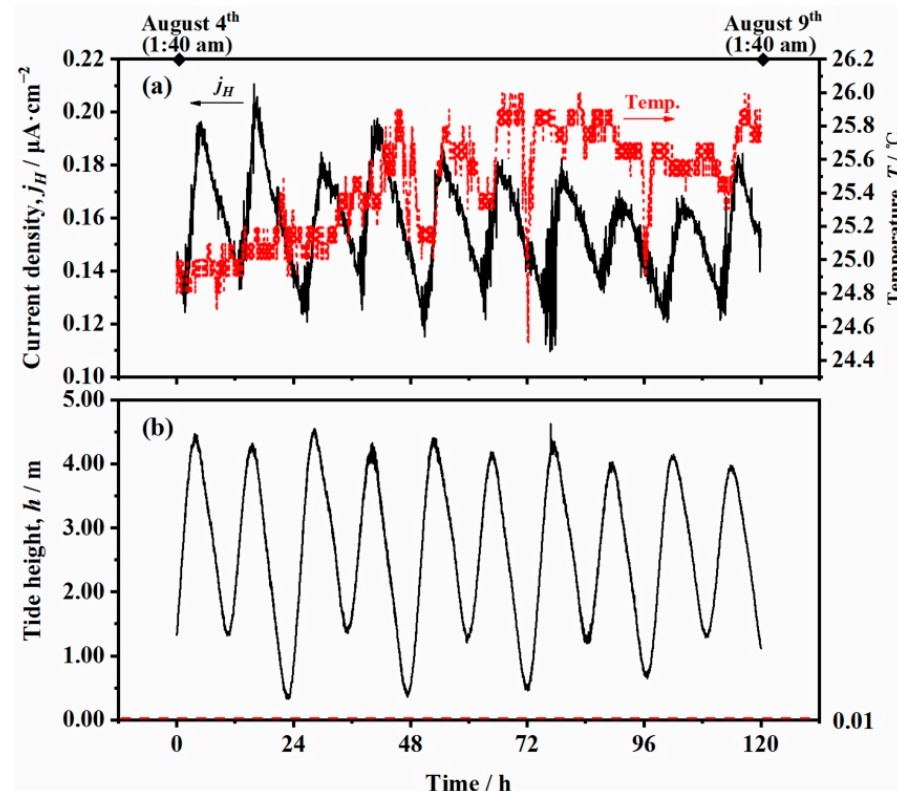


Figure 10. Time variations of the hydrogen permeation current density of the sensor exposed to the immersion zone and the corresponding temperature (a), as well as tidal changes (b), from 4 August to 9 August during outdoor hydrogen permeation test.

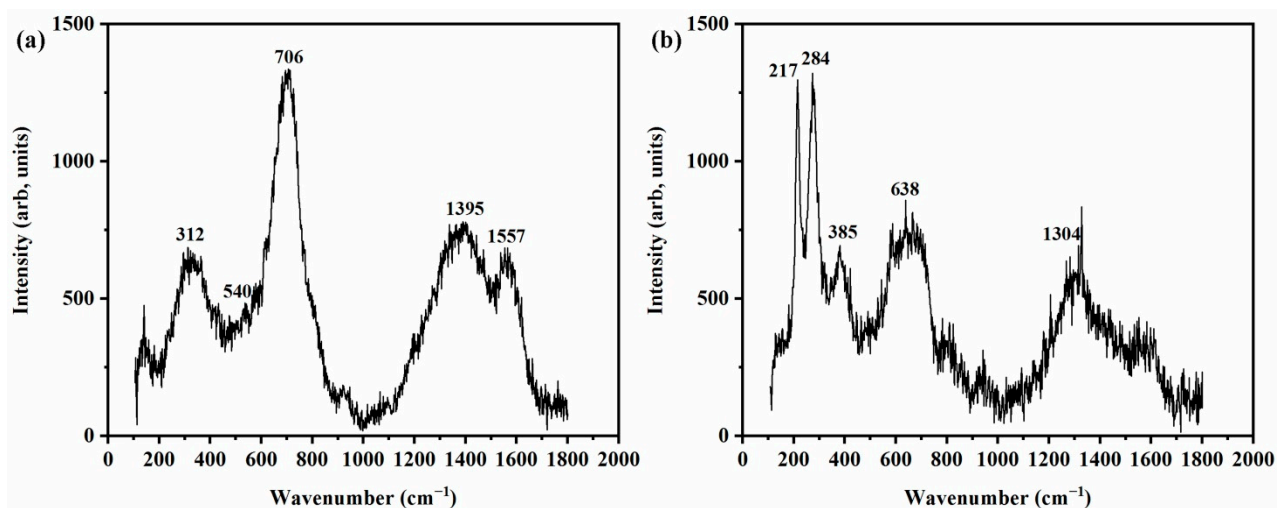


Figure 11. Raman spectra of the corrosion products formed on the surface of hydrogen permeation sensors exposed to the tidal zone (a) and the immersion zone (b).

It is considered that the sulfide products of SRB metabolic activity (S^{2-} , HS^- and H_2S) can act as a “catalyst” in facilitating hydrogen ions reduction and a “poisoning agent” in inhibiting hydrogen recombination, respectively, thus promoting hydrogen permeation into steels [44–46]. Many studies have reported the promoting effect of SRBs on hydrogen

permeation [47,48]. Zhu et al. [49] found that the hydrogen permeation current of steel in sea mud containing SRB was about three times to that in sterilized sea mud in the hydrogen permeation investigation of API X56 steel in sea mud. Furthermore, due to a large specific heat capacity of sea water, it was observed that changes in temperature of sea water in the immersion zone were very small and the maximum fluctuation range was about 2 °C. However, similarly, based on the background of a large hydrogen permeation current, the fluctuations of hydrogen permeation current caused by small changes in temperature can be obviously observed from Figure 10a.

3.1.2. The Relationship between Hydrogen Permeation and Corrosion Loss of Steel

The residual thickness of the side wall of the sensor was measured by using an optical microscope so as to obtain its thickness loss data, according to the method introduced in the published study [50]. The cross-sectional morphologies of the sensors endured corrosion exposure are shown in Figure S2 (refer to supplementary file). The widest and narrowest sites of corrosion residual thickness in each field of vision were selected for measurement, and the procedures were repeated for 72 times at different sites on the cross-section, as shown in Figure 12. After multiple measurements, the average corrosion thickness loss of the sensors in the marine atmospheric, splash, tidal and immersion zones are 54 μm , 245 μm , 127 μm and 230 μm , respectively. This result suggests that sensors in the splash and immersion zones have a higher corrosion rate in comparison with that of sensors in the marine atmospheric and tidal zones.

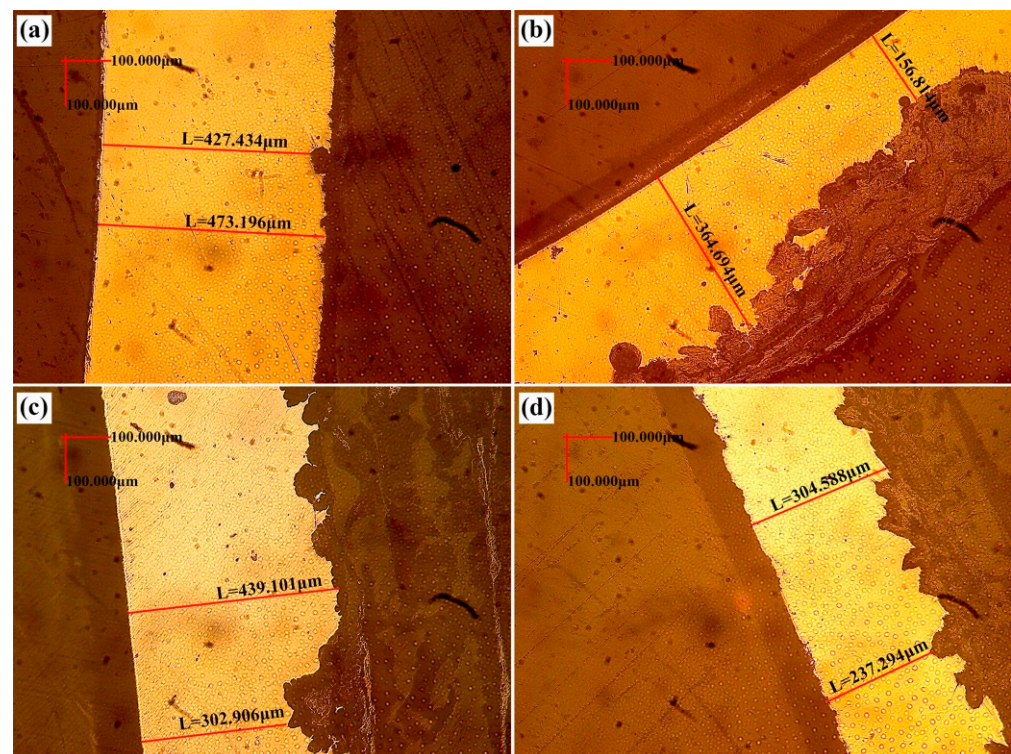


Figure 12. Residual thickness measurement on the cross-section of the sensors after being exposed for 3 months in the marine atmospheric zone (a), the splash zone (b), the tidal zone (c), and the immersion zone (d), respectively.

Hydrogen permeation behavior into the steel during exposure period was continuously monitored using electrochemical hydrogen permeation technique, as displayed in Figures 7–10. Based on the hydrogen permeation data continuously collected for 3 months,

the average hydrogen permeation current density (j_{aH}) and the sub-surface hydrogen concentration C_0 were calculated according to Equations (2)–(4):

$$Q_H = \int |i_H(t)| dt \quad (2)$$

$$j_{aH} = \frac{Q_H}{At} \quad (3)$$

$$C_0 = \frac{L \cdot i_{aH}}{n \cdot F \cdot D_{eff}} \quad (4)$$

where Q_H represents the quantity of hydrogen permeation charge, A is the total working area of the hydrogen permeation sensor, t is the corresponding test duration, L is the thickness of the steel specimen, F represents Faraday's constant with a value of 96,485 C/mol, n is number of transferred electrons in the hydrogen reduction reaction. Table 2 shows results of the j_{aH} and C_0 of steel in different marine corrosion zones. It can be found that the hydrogen permeation into steel in the splash zone is the most severe, while that of the steel in the atmospheric zone is the least. Meanwhile, the amount of the hydrogen permeated into the steel in the immersion zone is about 1.5 times that the hydrogen permeated into the steel in the tidal zone.

Table 2. The parameters for hydrogen permeation of AISI 4135 steel in different marine corrosion zones, including the average hydrogen permeation current density (j_{aH}), sub-surface hydrogen concentration (C_0), and diffusible hydrogen content (H_C).

Exposure Site	$j_{aH}/nA \cdot cm^{-2}$	$C_0/mol \cdot cm^{-3}$	$H_C/wt \text{ ppm}$
Atmospheric zone	19.6	2.46×10^{-8}	3.15×10^{-3}
Splash zone	435.3	5.46×10^{-7}	7.00×10^{-2}
Tidal zone	128.1	1.61×10^{-7}	2.06×10^{-2}
Immersion zone	206.9	2.60×10^{-7}	3.33×10^{-2}

Figure 13 shows the relationship between the time-averaged hydrogen permeation current density (i.e., j_{aH}) and the time-averaged corrosion thickness loss rate (r) of steels exposed to different marine corrosion zones. In Figure 13, it can be found that the average hydrogen permeation current density increases with the increase in corrosion thickness loss of steels. This suggests that hydrogen permeation into steel should be enhanced when the corrosion of steel is accelerated in the marine environment, which applies for all marine corrosion zones. The mechanisms of hydrogen embrittlement were summarized as internal pressure autocatalytic, Vacancy-Agglomeration and Lattice decohesion [51]. The hydrogen source is either internal or external. The low internal hydrogen concentration can be achieved by quality control of production. The hydrogen concentration dependence on corrosion rate indicates that the corrosion protection is an important way for hydrogen entry inhibition into steel. Earlier work showed that petrolatum tape cover was effective in inhibiting hydrogen entry under simulated marine splash conditions [52]. The validity of this technique for the hydrogen entry inhibition in other marine corrosion zones will be confirmed in future works.

3.1.3. Corrosion Products Analysis and Its Effect on Hydrogen Permeation

Different corrosive environments between marine corrosion zones may not only lead to differences in the corrosion rates of steel, but also differences in the composition of corrosion products. Figure 14 shows the XRD spectra of the corrosion products formed on the surface of sensors exposed to different marine corrosion zones. It can be seen that the corrosion products were mainly iron oxides, consisting of goethite (α -FeOOH), lepidocrocite (γ -FeOOH), akaganeite (β -FeOOH) and magnetite (Fe_3O_4). No sign of FeS was found in the XRD pattern of the corrosion products formed in the immersion zone, owing to the overlap of some peaks and less content. The XRD pattern shows a high

proportion of α -FeOOH in the corrosion products formed in the marine atmospheric zone. Previous studies have shown that a corrosion environment with a low content of chloride ions can facilitate the formation of α -FeOOH in the corrosion products, thus leading to a denser corrosion products layer. This dense corrosion products layer can largely hinder the penetration of O_2 and Cl^- to steel surface, thereby suppressing electrochemical corrosion and decreasing hydrogen permeation ultimately (Figure 7a) [53,54]. On the contrary, an environment with a high Cl^- content favors the formation of β -FeOOH [55,56] β -FeOOH can alter the structure of corrosion products layer such as facilitating the formation of cracks and pores, thereby promoting corrosion and hydrogen permeation into steel via providing extra channels for the penetration of corrosive substances [57]. Meanwhile, published studies have shown that the corrosion products layer formed on steel surface can suppress the anodic reaction of iron dissolution and simultaneously promote the hydrogen evolution reaction at the cathode, thus enhancing hydrogen permeation [58–60]. Furthermore, as mentioned above, corrosion product-FeS (as shown in Figure 11b) can simultaneously act as both “catalyst” and “poisoning agent” during hydrogen permeation process. Accordingly, the category of corrosion products can, in turn, affect the corrosion and hydrogen permeation behaviors of steel in a direct or indirect way.

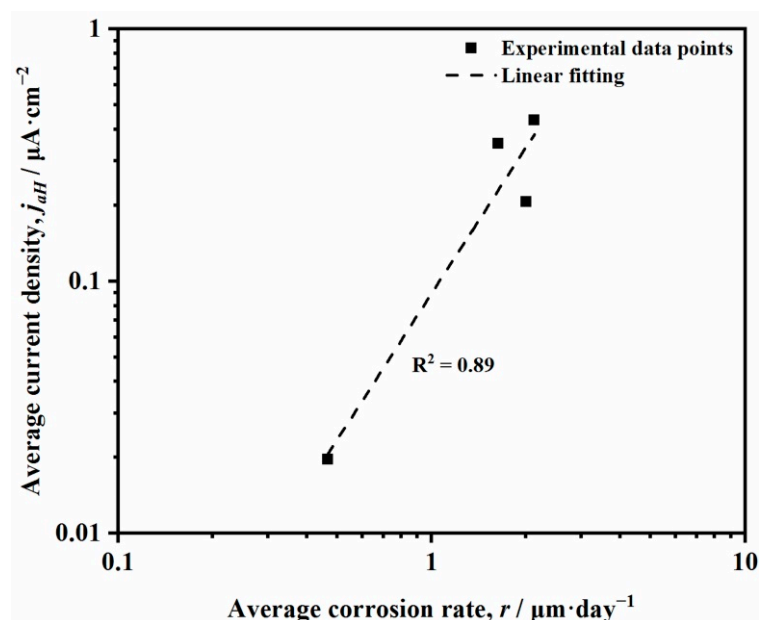


Figure 13. Relationship between the time-averaged hydrogen permeation current density (j_{aH}) and the time-averaged corrosion thickness loss rate (r) of the hydrogen permeation sensors in the entire duration of the outdoor hydrogen permeation test.

3.2. Hydrogen Permeation into Steel under the Simulated Wet–Dry Cycle Condition

It is observed from Figure 9 that the hydrogen permeation current does not vary monotonically during both the wetting and drying stages. To further verify the hydrogen permeation behavior of steels in the wet–dry cycle condition and investigate its mechanism, hydrogen permeation test was performed under the simulated wet–dry cycle condition. Figure 15a,b show the variations of the hydrogen permeation current density and open circuit potential of the sensor in laboratory simulated tidal cycling environment, respectively. Figure 15c shows changes in the indicator potential, indicating which state the hydrogen permeation sensor is in (wetting state or drying state). When the indicator potential shows 0 mV, it indicates that the sensor is in the drying state, otherwise the sensor is in the wetting state. It is found that changes in the hydrogen permeation current are nonmonotonic in the drying or wetting stages (Figure 15a). During the drying stage, the hydrogen permeation current firstly decreased and then increased, while during the wetting stage, it showed the

opposite characterization. In addition, it is obvious that the overall hydrogen permeation current in the wetting stage is higher than that during the drying stage, which is consistent with the outdoor experiment results (Figure 9).

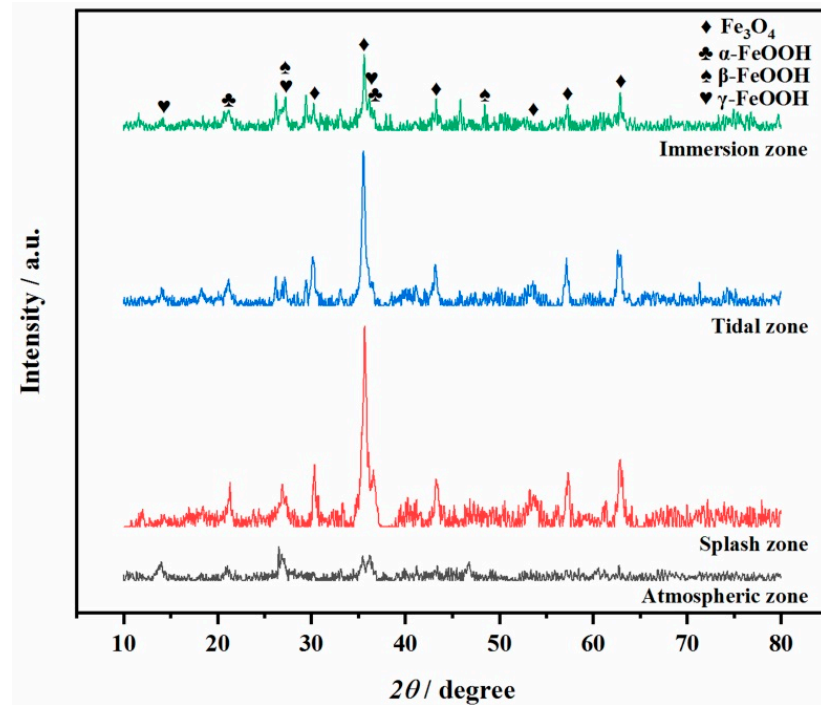


Figure 14. XRD spectra of the corrosion products formed on the surface of sensors exposed to different marine corrosion zones.

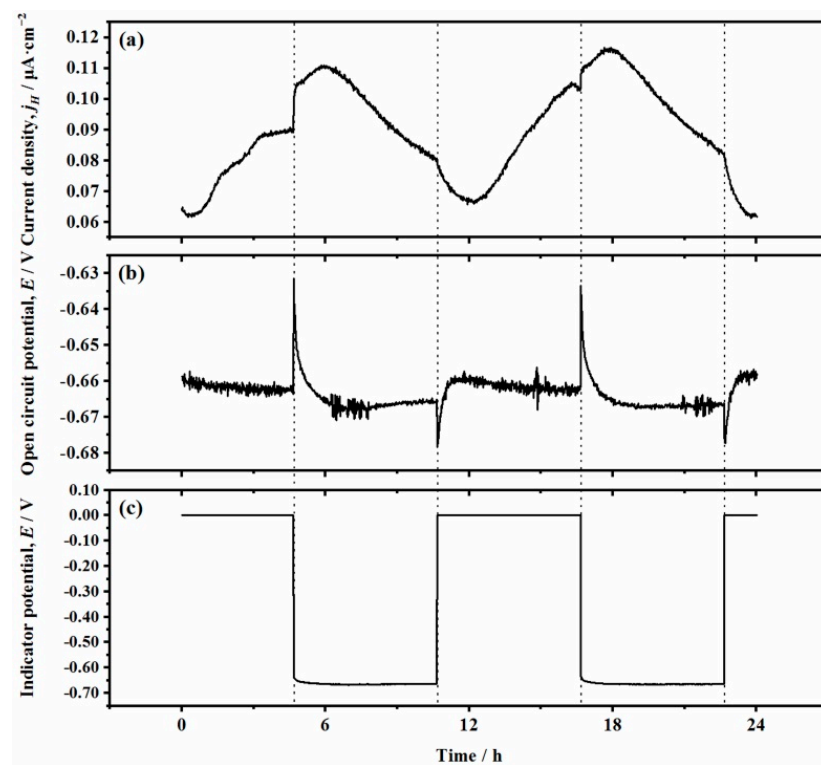
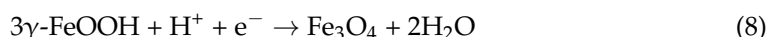
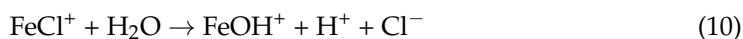
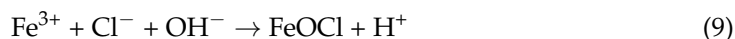


Figure 15. Variations of the hydrogen permeation current density (a) and open circuit potential (b) of the sensor, and indicator potential (c) under the simulated wet–dry cycle condition.

Under the wet–dry cycle condition, the anodic dissolution of iron during the electrochemical corrosion process can be balanced by the hydrogen reduction reaction Equation (5), the dissolved oxygen reduction reaction Equation (6) and the reduction reactions of corrosion products represented by Equations (7) and (8) [61–63]:



Under the wet–dry cycle condition, the dominant cathodic reactions of steel corrosion in different states possess some differences. Evans [64] and Stratmann et al. [65,66] proposed that the corrosion process of steel in the simulated atmospheric corrosion environment can be divided into three stages: wetting of the dry surface, wet surface and drying-out of the surface. Meanwhile, they found that the cathodic reduction reactions of ferric species within the corrosion products were significantly enhanced when the oxygen reduction reaction was weakened in the wetting stage, whereas the oxygen reduction reaction was dominant in the wet stage. During tidal cycles, the oxygen is prone to diffuse through a thin electrolyte film to steel surface when it is exposed to atmosphere. In this case, the oxygen reduction reaction (Equation (6)) and ferric species reduction reactions (Equations (7) and (8)) are dominant in cathodic reactions. However, this does not mean that hydrogen reduction reaction (Equation (5)) is inactive in this stage, in fact the opposite is true, because the hydrolysis of corrosion products can result in acidification of the electrolyte beneath the rust layer (Equations (9) and (10)). Meanwhile, the acidity of the electrolyte is further enhanced with the evaporation of water during exposure, the pH value of which can be even lower than 3 with the presence of chloride ions [11,67].



Based on Nernst equation, the equilibrium potential of the hydrogen evolution reaction at 25 °C can be expressed as:

$$E_{\text{H}_2/\text{H}^+} = -0.0591\text{pH} \quad (11)$$

The equilibrium potential of the hydrogen evolution reaction in natural seawater (pH = 7.5) is about $-0.684 \text{ V}_{\text{SCE}}$, whereas it is only $-0.177 \text{ V}_{\text{SCE}}$ when the pH of the electrolyte under the rust layer drops to 3 during the drying stage. It is seen from Figure 15c that the value of the OCP of steel is about $-0.66 \text{ V}_{\text{SCE}}$ during the drying stage. Therefore, a lower OCP and pH during the middle and late drying stage can enhance the activity of the hydrogen evolution reaction, thereby resulting in a higher hydrogen permeation current, as shown in Figure 15a. However, the pH of the electrolyte beneath the rust layer is still high in the initial drying stage, which brings difficulties to the hydrogen evolution owing to a higher overpotential, thus leading to the persistent decrease in the hydrogen permeation current. Accordingly, cathodic reactions (Equations (5)–(8)) can actively proceed in the drying stage during the tidal cycles, although the contribution of the hydrogen reduction reaction to corrosion weight loss of steels may be only about 0.1% [11].

In contrast, the pH of the electrolyte beneath the rust layer is basically the same as that of sea water owing to the good ion transport between sea water and the electrolyte beneath the rust layer. Therefore, hydrogen evolution under immersion condition is more difficult to proceed in the case where the OCP of the steel is almost equal during the drying and wetting stages. This reasonably explains the continuous decrease in the hydrogen permeation current in the middle and the last wetting stages. Meanwhile, the supply of oxygen to the surface of the rusty steel is insufficient in the wetting stage. This can be attributed to two aspects. On one hand, the steel surface left in contact with electrolyte by the rust layer is very small, limiting substances exchange. On the other hand, tortuous

pores of nanometric width in the thick rust layer add more difficulty to the diffusion of oxygen. Therefore, the corrosion of the steel is relatively mild in the wetting stage, and the corrosion process is controlled by the diffusion of dissolved oxygen [68]. Therefore, the lower corrosion rate of the steel is also another reason for the lower hydrogen permeation current in the wetting stage. Meanwhile, it is also due to the temporary inhibition of the rust layer on the diffusion of hydrogen ions, which causes the brief rise in the hydrogen permeation current at the initial wetting stage, as shown in Figure 15.

4. Conclusions

Hydrogen permeation behavior and the mechanism of AISI 4135 steel in different marine corrosion zones were investigated using an in situ hydrogen permeation monitoring system via outdoor and indoor hydrogen permeation tests. The conclusions can be summarized as follows:

- (1) A good performance of the in situ hydrogen permeation monitoring system was present in both the outdoor and indoor hydrogen permeation tests. Hydrogen permeation into steel during corrosion in different marine corrosion zones can be evaluated with good accuracy through the collected hydrogen permeation current data during outdoor testing.
- (2) The 3-month outdoor hydrogen permeation tests showed that the diffusible hydrogen content of steels in the marine atmospheric, splash, tidal and immersion zones were 3.15×10^{-3} , 7.00×10^{-2} , 2.06×10^{-2} and 3.33×10^{-2} wt ppm, respectively.
- (3) It was found that the hydrogen permeation current density is positively correlated with the corrosion rate of the steel in the marine environment. A large hydrogen permeation current of the steel exposed to the immersion zone was observed during the outdoor test, which is considered to be related to the formation of FeS in the corrosion products caused by SRB.
- (4) There are no obvious changes in the OCP of the steel during tidal cycles, and the change in the hydrogen permeation current is mainly controlled by the pH of electrolyte and oxygen concentration beneath the rust layer.

Supplementary Materials: The following supporting information can be downloaded at: <https://www.mdpi.com/article/10.3390/app12062785/s1>, Figure S1: Details of dimensional information for metal specimens; Figure S2: Macro-morphologies on the cross-section of the sensors after exposure in the atmospheric zone (a), the splash zone (b), the tidal zone (c), and the immersion zone (d), respectively.

Author Contributions: Data curation, Y.X.; Formal analysis, D.L.; Funding acquisition, Y.H.; Methodology, L.Y.; Project administration, Y.H.; Software, F.C.; Validation, Z.W.; Writing—original draft, Y.X.; Writing—review & editing, X.W. All authors have read and agreed to the published version of the manuscript.

Funding: This work was financially supported by the National Natural Science Foundation of China under Grant <No. 41976033>.

Data Availability Statement: The raw data related to this manuscript will be made available on request.

Conflicts of Interest: The authors declare no conflict of interest.

References

1. Omura, T. Hydrogen entry and its effect on delayed fracture susceptibility of high strength steel bolts under atmospheric corrosion. *ISIJ Int.* **2012**, *52*, 267–273. [[CrossRef](#)]
2. Nanninga, N.E.; Levy, Y.S.; Drexler, E.S.; Condon, R.T.; Stevenson, A.E.; Slifka, A.J. Comparison of hydrogen embrittlement in three pipeline steels in high pressure gaseous hydrogen environments. *Corros. Sci.* **2012**, *59*, 1–9. [[CrossRef](#)]
3. Venezuela, J.; Liu, Q.; Zhang, M.; Zhou, Q.; Atrens, A. The influence of hydrogen on the mechanical and fracture properties of some martensitic advanced high strength steels studied using the linearly increasing stress test. *Corros. Sci.* **2015**, *99*, 98–117. [[CrossRef](#)]
4. Wang, M.Q.; Akiyama, E.; Tsuzaki, K. Effect of hydrogen and stress concentration on the notch tensile strength of AISI 4135 steel. *Mater. Sci. Eng. A* **2005**, *398*, 37–46. [[CrossRef](#)]

5. Liu, Z.Y.; Hao, W.K.; Wu, W.; Luo, H.; Li, X.G. Fundamental investigation of stress corrosion cracking of E690 steel in simulated marine thin electrolyte layer. *Corros. Sci.* **2019**, *148*, 388–396. [[CrossRef](#)]
6. Li, S.; Akiyama, E.; Uno, N.; Hirai, K.; Tsuzaki, K.; Zhang, B. Evaluation of delayed fracture property of outdoor-exposed high strength AISI 4135 steels. *Corros. Sci.* **2010**, *52*, 3198–3204. [[CrossRef](#)]
7. Wei, H.; Chen, Y.L.; Yu, W.; Su, L.; Wang, X.; Tang, D. Study on corrosion resistance of high-strength medium-carbon spring steel and its hydrogen-induced delayed fracture. *Constr. Build. Mater.* **2020**, *239*, 117815. [[CrossRef](#)]
8. Hirth, J.P. Effects of hydrogen on the properties of iron and steel. *Metall. Mater. Trans. A* **1980**, *11*, 861–890. [[CrossRef](#)]
9. Omura, T.; Kudo, T.; Fujimoto, S. Environmental factors affecting hydrogen entry into high strength steel due to atmospheric corrosion. *Mater. Trans.* **2006**, *47*, 2956–2962. [[CrossRef](#)]
10. Tsuru, T.; Huang, Y.L.; Ali, M.R.; Nishikata, A. Hydrogen entry into steel during atmospheric corrosion process. *Corros. Sci.* **2005**, *47*, 2431–2440. [[CrossRef](#)]
11. Huang, Y.L.; Zhu, Y.Y. Hydrogen ion reduction in the process of iron rusting. *Corros. Sci.* **2005**, *47*, 1545–1554. [[CrossRef](#)]
12. Yu, Q.; Huang, Y.L.; Zheng, C. Hydrogen permeation and corrosion behaviour of high strength steel 35CrMo under cyclic wet-dry conditions. *Corros. Eng. Sci. Technol.* **2008**, *43*, 241–247. [[CrossRef](#)]
13. Ootsuka, S.; Fujita, S.; Tada, E.; Nishikata, A.; Tsuru, T. Evaluation of hydrogen absorption into steel in automobile moving environments. *Corros. Sci.* **2015**, *98*, 430–437. [[CrossRef](#)]
14. Akiyama, E.; Matsukado, K.; Wang, M.Q.; Tsuzaki, K. Evaluation of hydrogen entry into high strength steel under atmospheric corrosion. *Corros. Sci.* **2010**, *52*, 2758–2765. [[CrossRef](#)]
15. Nishimura, R.; Shiraishi, D.; Maeda, Y. Hydrogen permeation and corrosion behavior of high strength steel MCM 430 in cyclic wet-dry SO₂ environment. *Corros. Sci.* **2004**, *46*, 225–243. [[CrossRef](#)]
16. Ootsuka, S.; Tada, E.; Ooi, A.; Nishikata, A. Effect of environmental factors on hydrogen absorption into steel sheet under a wet-dry cyclic corrosion condition. *ISIJ Int.* **2020**, *106*, 448–456. [[CrossRef](#)]
17. Hagihara, Y.; Ito, C.; Hisamori, N.; Suzuki, H.; Takai, K.; Akiyama, E. Evaluation of delayed fracture characteristics of high strength steel based on CSRT method. *ISIJ Int.* **2008**, *94*, 215–221. [[CrossRef](#)]
18. Takai, K.; Seki, J.; Homma, Y. Hydrogen occlusion behavior during delayed fracture in cold drawn steel wire and heat-treated steel bar for prestressed concrete. *ISIJ Int.* **1995**, *81*, 1025–1030. [[CrossRef](#)]
19. Omura, T.; Matsumoto, H.; Hasegawa, T.; Miyakoshi, Y. Effects of Alloying Elements on Hydrogen Entry to Low Alloy Steels under a Cyclic Corrosion Condition. *ISIJ Int.* **2016**, *56*, 385–391. [[CrossRef](#)]
20. Kobayashi, K.; Omura, T.; Fujimoto, S. Effects of environmental factors on hydrogen absorption and sulfide stress cracking susceptibility of low alloy steel. *Corrosion* **2020**, *76*, 698–706. [[CrossRef](#)]
21. Kushida, T. Hydrogen entry into steel by atmospheric corrosion. *ISIJ Int.* **2003**, *43*, 470–474. [[CrossRef](#)]
22. Dey, S.; Mandhyan, A.K.; Sondhi, S.K.; Chattoraj, I. Hydrogen entry into pipeline steel under freely corroding conditions in two corroding media. *Corros. Sci.* **2006**, *48*, 2676–2688. [[CrossRef](#)]
23. Azevedo, C.; Bezerra, P.S.A.; Esteves, F.; Joia, C.; Mattos, O.R. Hydrogen permeation studied by electrochemical techniques. *Electrochim. Acta* **1999**, *44*, 4431–4442. [[CrossRef](#)]
24. Gajek, A.; Wolarek, Z.; Zakroczymski, T. Behaviour of hydrogen in gas nitrated iron studied by electrochemical permeation and desorption techniques. *Corros. Sci.* **2012**, *58*, 260–266. [[CrossRef](#)]
25. Manolatos, P.; Durethual, C.; Lecoze, J.; Jerome, M. The electrochemical permeation of hydrogen in palladium: Boundary conditions during a galvanostatic charging under low charging current densities. *Corros. Sci.* **1995**, *37*, 1797–1807. [[CrossRef](#)]
26. Manolatos, P.; Jerome, M.; Durethual, C.; Lecoze, J. The electrochemical permeation of hydrogen in steels without palladium coating. Part I: Interpretation difficulties. *Corros. Sci.* **1995**, *37*, 1773–1783. [[CrossRef](#)]
27. Manolatos, P.; Durethual, C.; Lecoze, J.; Jerome, M.; Bollinger, E. The electrochemical permeation of hydrogen in steels without palladium coating. Part II. Study of the influence of microstructure on hydrogen diffusion. *Corros. Sci.* **1995**, *37*, 1785–1796. [[CrossRef](#)]
28. Husby, H.; Iannuzzi, M.; Johnsen, R.; Kappes, M.; Barnoush, A. Effect of nickel on hydrogen permeation in ferritic/pearlitic low alloy steels. *Int. J. Hydrogen Energy* **2018**, *43*, 3845–3861. [[CrossRef](#)]
29. Devanathan, M.A.V.; Stachurski, Z. The adsorption and diffusion of electrolytic hydrogen in palladium. *Proc. R. Soc. A* **1962**, *270*, 90–102. [[CrossRef](#)]
30. Perme, S.; Lau, K.; Boan, M.E.; Tansel, B.; Duncan, M. Cathodic polarization behavior of steel with different marine fouling morphologies on submerged bridge elements with cathodic protection. *J. Mater. Civ. Eng.* **2020**, *32*, 04020184. [[CrossRef](#)]
31. de Messano, L.V.R.; Sathler, L.; Reznik, L.Y.; Coutinho, R. The effect of biofouling on localized corrosion of the stainless steels N08904 and UNS S32760. *Int. Biodeterior. Biodegrad.* **2009**, *63*, 607–614. [[CrossRef](#)]
32. de Messano, L.V.R.; Reznik, L.Y.; Sathler, L.; Coutinho, R. Evaluation of biocorrosion on stainless steels using laboratory-reared barnacle *Amphibalanus amphitrite*. *Anti-Corros. Methods Mater.* **2014**, *61*, 402–408. [[CrossRef](#)]
33. De Brito, L.V.R.; Coutinho, R.; Cavalcanti, E.S.; Benchimol, M. The influence of macrofouling on the corrosion behaviour of API 5L X65 carbon steel. *Biofouling* **2007**, *23*, 193–201. [[CrossRef](#)] [[PubMed](#)]
34. Palanichamy, S.; Subramanian, G.; Eashwar, M. Corrosion behaviour and biofouling characteristics of structural steel in the coastal waters of the Gulf of Mannar (Bay of Bengal), India. *Biofouling* **2012**, *28*, 441–451. [[CrossRef](#)] [[PubMed](#)]

35. Yang, K.J.; Liu, Y.L.; Liu, N.; Shao, P.; Zhang, X.; Ma, Y. Hydrogen transport in tungsten for nuclear energy application: Temperature dependence and compensation effect. *Fusion Sci. Technol.* **2020**, *76*, 616–631. [[CrossRef](#)]
36. Zheng, C.; Yi, G.; Gao, Y. An electrochemical sensor for measuring hydrogen permeation behavior in atmospheric environment. *Int. J. Electrochem. Sci.* **2012**, *7*, 9518–9525.
37. Saeedikhani, M.; Van den Steen, N.; Wijesinghe, S.; Vafakhah, S.; Terryn, H.; Blackwood, D.J. Moving Boundary Simulation of Iron-Zinc Sacrificial Corrosion under Dynamic Electrolyte Thickness Based on Real-Time Monitoring Data. *J. Electrochem. Soc.* **2020**, *167*, 041503. [[CrossRef](#)]
38. Hou, B.R.; Zhang, J.L.; Sun, H.Y.; Li, Y.; Xiang, B. Corrosion of C-Mn steel in simulated tidal and immersion zones. *Brit. Corros. J.* **2001**, *36*, 310–312. [[CrossRef](#)]
39. Wang, H.H.; Du, M. Corrosion behavior of a low-carbon steel in simulated marine splash zone. *Acta Metall. Sin.* **2017**, *30*, 585–593. [[CrossRef](#)]
40. Bourdoiseau, J.A.; Jeannin, M.; Sabot, R.; Remazeilles, C.; Refait, P. Characterisation of mackinawite by Raman spectroscopy: Effects of crystallisation, drying and oxidation. *Corros. Sci.* **2008**, *50*, 3247–3255. [[CrossRef](#)]
41. Pineau, S.; Sabot, R.; Quillet, L.; Jeannin, M.; Caplat, C.; Dupont-Morrall, I.; Refait, P. Formation of the Fe(II-III) hydroxysulphate green rust during marine corrosion of steel associated to molecular detection of dissimilatory sulphite-reductase. *Corros. Sci.* **2008**, *50*, 1099–1111. [[CrossRef](#)]
42. Refait, P.; Nguyen, D.D.; Jeannin, M.; Sable, S.; Langumier, M.; Sabot, R. Electrochemical formation of green rusts in deaerated seawater-like solutions. *Electrochim. Acta* **2011**, *56*, 6481–6488. [[CrossRef](#)]
43. Alcantara, J.; Chico, B.; Simancas, J.; Diaz, I.; de la Fuente, D.; Morcillo, M. An attempt to classify the morphologies presented by different rust phases formed during the exposure of carbon steel to marine atmospheres. *Mater. Charact.* **2016**, *118*, 65–78. [[CrossRef](#)]
44. Robinson, M.J.; Kilgallon, P.J. Hydrogen embrittlement of cathodically protected high-strength, low-alloy steels exposed to sulfate-reducing bacteria. *Corrosion* **1994**, *50*, 626–635. [[CrossRef](#)]
45. Newman, J.F.; Shreir, L.L. Role of hydrides in hydrogen entry into steel from solutions containing promoters. *Corros. Sci.* **1969**, *9*, 631–641. [[CrossRef](#)]
46. de Moraes, F.D.; Bastian, F.L.; Ponciano, J.A. Influence of dynamic straining on hydrogen embrittlement of UNS-G41300 and UNS-S31803 steels in a low H₂S concentration environment. *Corros. Sci.* **2005**, *47*, 1325–1335. [[CrossRef](#)]
47. Wu, T.; Yan, C.; Zeng, D.; Xu, J.; Sun, C.; Yu, C.; Ke, W. Hydrogen permeation of X80 steel with superficial stress in the presence of sulfate-reducing bacteria. *Corros. Sci.* **2015**, *91*, 86–94. [[CrossRef](#)]
48. Lv, M.; Chen, X.; Li, Z.; Du, M. Effect of sulfate-reducing bacteria on hydrogen permeation and stress corrosion cracking behavior of 980 high-strength steel in seawater. *J. Mater. Sci. Technol.* **2021**, *92*, 109–119. [[CrossRef](#)]
49. Zhu, Y.; Huang, Y.; Zheng, C.; Yu, Q. The hydrogen permeation investigation of API X56 steel in sea mud. *Mater. Corros.* **2007**, *58*, 447–451. [[CrossRef](#)]
50. Marty, F.; Gueune, H.; Malard, E.; Sanchez-Amaya, J.M.; Sjogren, L.; Abbas, B.; Quillet, L.; van Loosdrecht, M.C.M.; Muyzer, G. Identification of key factors in Accelerated Low Water Corrosion through experimental simulation of tidal conditions: Influence of stimulated indigenous microbiota. *Biofouling* **2014**, *30*, 281–297. [[CrossRef](#)]
51. Nagumo, M. Hydrogen related failure of steels—A new aspect. *Mater. Sci. Technol.* **2004**, *20*, 940–950. [[CrossRef](#)]
52. Qu, W.; Huang, Y.; Yu, X.; Zheng, M.; Lu, D. Effect of Petrolatum Tape Cover on the Hydrogen Permeation of Al-Si4135 Steel under Marine Splash Zone Conditions. *Int. J. Electrochem. Sci.* **2015**, *10*, 5892–5904.
53. Asami, K.; Kikuchi, M. In-depth distribution of rusts on a plain carbon steel and weathering steels exposed to coastal-industrial atmosphere for 17 years. *Corros. Sci.* **2003**, *45*, 2671–2688. [[CrossRef](#)]
54. Fan, Y.M.; Liu, W.; Li, S.M.; Chowwanonthapunya, T.; Wongpat, B.; Zhao, Y.G.; Dong, B.J.; Zhang, T.Y.; Li, X.G. Evolution of rust layers on carbon steel and weathering steel in high humidity and heat marine atmospheric corrosion. *J. Mater. Sci. Technol.* **2020**, *39*, 190–199. [[CrossRef](#)]
55. Ma, Y.T.; Li, Y.; Wang, F.H. The effect of beta-FeOOH on the corrosion behavior of low carbon steel exposed in tropic marine environment. *Mater. Chem. Phys.* **2008**, *112*, 844–852. [[CrossRef](#)]
56. Remazeilles, C.; Refait, P. On the formation of beta-FeOOH (akaganeite) in chloride-containing environments. *Corros. Sci.* **2007**, *49*, 844–857. [[CrossRef](#)]
57. Stahl, K.; Nielsen, K.; Jiang, J.Z.; Lebech, B.; Hanson, J.C.; Norby, P.; van Lanschot, J. On the akaganeite crystal structure, phase transformations and possible role in post-excavational corrosion of iron artifacts. *Corros. Sci.* **2003**, *45*, 2563–2575. [[CrossRef](#)]
58. Ma, Y.; Li, Y.; Wang, F. Weatherability of 09CuPCrNi steel in a tropical marine environment. *Corros. Sci.* **2009**, *51*, 1725–1732. [[CrossRef](#)]
59. Shi, J.; Ming, J.; Zhang, Y.; Jiang, J. Corrosion products and corrosion-induced cracks of low-alloy steel and low-carbon steel in concrete. *Cem. Concr. Compos.* **2018**, *88*, 121–129. [[CrossRef](#)]
60. Gong, K.; Wu, M.; Xie, F.; Liu, G.; Sun, D. Effect of Cl⁻ and rust layer on stress corrosion cracking behavior of X100 steel base metal and heat-affected zone in marine alternating wet/dry environment. *Mater. Chem. Phys.* **2021**, *270*, 124826. [[CrossRef](#)]
61. Cox, A.; Lyon, S.B. An electrochemical study of the atmospheric corrosion of iron—2. Cathodic and anodic processes on uncorroded and pre-corroded iron. *Corros. Sci.* **1994**, *36*, 1177–1192. [[CrossRef](#)]

62. Stratmann, M.; Hoffmann, K. In situ mossbauer spectroscopic study of reactions within rust layers. *Corros. Sci.* **1989**, *29*, 1329–1352. [[CrossRef](#)]
63. Kuch, A. Investigations of the reduction and reoxidation kinetics of iron (III) oxide scales formed in waters. *Corros. Sci.* **1988**, *28*, 221–231. [[CrossRef](#)]
64. Evans, U.R. Mechanism of rusting. *Corros. Sci.* **1969**, *9*, 813. [[CrossRef](#)]
65. Stratmann, M. The investigation of the corrosion properties of metals, covered with adsorbed electrolyte layers-A new experimental technique. *Corros. Sci.* **1987**, *27*, 869–872. [[CrossRef](#)]
66. Stratmann, M.; Streckel, H. On the atmospheric corrosion of metals which are covered with thin electrolyte layers. 1. Verification of the experimental technique. *Corros. Sci.* **1990**, *30*, 681–696. [[CrossRef](#)]
67. Venezuela, J.; Zhou, Q.J.; Liu, Q.L.; Zhang, M.X.; Atrens, A. Influence of hydrogen on the mechanical and fracture properties of some martensitic advanced high strength steels in simulated service conditions. *Corros. Sci.* **2016**, *111*, 602–624. [[CrossRef](#)]
68. Gong, K.; Wu, M.; Liu, G.X. Comparative study on corrosion behaviour of rusted X100 steel in dry/wet cycle and immersion environments. *Constr. Build. Mater.* **2020**, *235*, 117440. [[CrossRef](#)]